

Deep Joint CSI Estimation-Feedback-Precoding for MU-MIMO OFDM Systems

Yiran Guo, Wei Chen, *Senior Member, IEEE*, Bo Ai, *Fellow, IEEE*, Lun Li

Abstract—As the number of antennas in frequency-division duplex (FDD) multiple-input multiple-output (MIMO) systems increases, acquiring channel state information (CSI) becomes increasingly challenging due to limited spectral resources and feedback overhead. In this paper, we propose an end-to-end network that conducts joint design with pilot design, CSI estimation, CSI feedback, and precoding design in the multi-user MIMO orthogonal frequency-division multiplexing (OFDM) scenario. Multiple communication modules are jointly designed and trained with a common optimization objective to prevent mismatches between modules and discrepancies between individual module objectives and the final system goal. Experimental results demonstrate that, under the same feedback and CE overheads, the proposed joint multi-module end-to-end network achieves a higher multi-user downlink spectral efficiency than traditional algorithms based on separate architecture and partially separated artificial intelligence-based network architectures under comparable channel quality. Furthermore, compared to conventional separate architecture, the proposed network architecture with joint architecture reduces the computational burden and model storage overhead at the UE side, facilitating the deployment of low-overhead multi-module joint architectures in practice. While slightly increasing storage requirements at the base station, it reduces computational complexity and precoding design delay, effectively reducing the effects of channel aging challenges.

Index Terms—CSI feedback, precoding design, CSI estimation, deep joint source-channel coding.

I. INTRODUCTION

With the significant performance improvements brought by massive multiple-input multiple-output (MIMO) technology in 5G systems, and the growing demands for higher spectrum utilization, increased communication throughput, and faster transmission rates in the vision of 6G [1], MIMO technology and its evolving variants are expected to become key technologies for 6G. The development of MIMO technology, such as extremely large-scale MIMO [2] and reconfigurable intelligent surface [3] technologies, offers valuable insights into the application of MIMO in 6G systems. Additionally, research into terahertz band communication [4] provides theoretical support for MIMO systems that can accommodate more antennas and more effectively exploit spatial resources. However, to fully harness the potential of MIMO technology, obtaining channel state information (CSI) with low overhead is a critical challenge. In time-division duplex (TDD) systems, channel reciprocity between uplink and downlink channels

operating in the same frequency band simplifies downlink CSI acquisition. Conversely, in frequency-division duplex (FDD) systems, where channel reciprocity is weak, the increased number of antennas presents significant challenges for downlink CSI estimation and feedback with low overhead and low latency.

Traditional methods for CSI feedback include the codebook-based feedback method, commonly applied in 5G, and the compressed sensing (CS) method based on sparsity assumptions [5]. However, the codebook-based feedback approach faces scalability challenges as the number of antennas increases. Ensuring the same reconstruction accuracy requires a larger codebook size, leading to increased complexity in codeword search and higher feedback overhead. Similarly, the CS-based CSI feedback method is constrained by the sparsity assumption, making it difficult to achieve theoretical performance. Additionally, the complex reconstruction algorithms in CS methods introduce significant computational overhead and delay, making them unsuitable for fast time-varying channels prone to CSI aging.

With the promising performance of artificial intelligence (AI) techniques in fields such as image compression and transmission [6], and signal processing [7], AI-based methods are increasingly adopted for communication tasks, particularly CSI feedback [8], [9]. These methods treat the CSI as an image, where the real and imaginary components are considered as separate channels. AI-based techniques exploit the correlation of CSI in the frequency and spatial domains to compress high-dimensional CSI into low-dimensional feature vectors using an auto-encoder at the transmitter. The compressed features are fed back, and the CSI is reconstructed at the receiver using a corresponding decoder. This CSI feedback process is considered an image compression and reconstruction task, trained end-to-end from user equipment (UE) to the base station (BS), with reconstruction accuracy as the optimization objective to update trainable parameters. By replacing traditional source coding and decoding modules with AI-based compression and reconstruction modules, various network architectures have been proposed to achieve low-overhead, high-accuracy CSI feedback, addressing key limitations of traditional methods [10]–[12].

The use of AI networks to replace traditional source coding and decoding modules in communication architectures is referred to as a separate source-channel coding (SSCC) architecture. In this approach, the design of the separate architecture allows the network to be trained without considering the impact of channel coding and decoding on performance, which results in the network performance being highly affected by channel quality. In contrast, the authors of [13] proposed

Yiran Guo, Wei Chen and Bo Ai are with the School of Electronic and Information Engineering, Beijing Jiaotong University, China. (Corresponding author: Wei Chen.) Lun Li is with the State Key Laboratory of Mobile Network and Mobile Multimedia, Shenzhen, China, and ZTE Corporation, Nanshan District, Shenzhen 518055, China.

This work is supported by ZTE Industry-University-Institute Cooperation Funds under Grant No. IA20240420002.

a deep joint source-channel coding (DJSCC) architecture for CSI feedback, which jointly considers source coding, channel coding, channel decoding, and source decoding. This approach abandons the traditionally modular design seen in communication systems. By leveraging the powerful nonlinear capabilities of AI, the DJSCC module provides more stable and reliable CSI reconstruction performance compared to the SSCC architecture.

The challenges encountered by separate architectures also arise in both the upstream task (CSI estimation) and the downstream task (precoding design) of CSI feedback. Inaccurate CSI estimation can cause a mismatch in the input distribution of the CSI compression module between the training and testing phases, leading to inaccurate CSI feedback. In our previous work [14], we explored several joint multi-module end-to-end networks for the CSI feedback task, demonstrating the benefits of joint multi-module design. In [10], [11], [15], AI-based two-sided CSI compression and reconstruction modules are designed and jointly trained to perform the CSI feedback task, typically resulting in improved CSI reconstruction performance compared to one-sided feedback architectures in [8], [16], [17] and codebook-based feedback architectures in traditional algorithms. In [13], the CSI compression and reconstruction module is jointly designed with the channel coding and decoding module to mitigate the “cliff effect” and reduce retransmission delays. In our previous work [18], we proposed a joint feedback and precoding network (JFPNet) for multi-user (MU) MIMO scenarios that simultaneously addresses both CSI feedback and its downstream task, precoding design. The source coding and channel coding modules are jointly designed on the UE side, while the channel decoding, source decoding, and precoding design modules for MU scenarios are jointly designed on the BS side. According to the experimental results in [18], this joint multi-module architecture outperforms the separate architecture for the CSI feedback and precoding design task. In [19], an end-to-end multi-module joint architecture was designed to simultaneously address upstream and downstream tasks, including pilot length design, CE, CSI feedback, and beamforming precoding. However, its pilot sequences are randomly generated from a complex unit sphere, limiting the ability to fully utilize channel information and exploit the learning capacity of the end-to-end architecture. Additionally, its downlink CE process relies on artificially introduced noise to simulate CE errors, which are inconsistent with the actual errors caused by specific CE methods, resulting in performance degradation. Both the joint CSI feedback and estimation architecture in [20] and the joint CSI estimation, feedback, and precoding design architecture in [21], [22] address the end-to-end performance loss caused by mismatches between the distribution of the estimated and trained CSI. However, both overlook the potential “cliff effect” caused by the omission of channel coding and decoding, as well as the added retransmission overhead and delay when channel quality degrades.

To address this gap, we propose a joint CSI estimation, feedback, and precoding design network (JEFPNet). In summary, our contributions to this work are as follows:

- In a MU MIMO-OFDM system, we propose an end-

to-end network that jointly addresses CSI feedback, its upstream task (CSI estimation), and its downstream task (precoding design). The proposed framework considers the entire closed-loop system, starting from the pilot design at the BS, to the CSI estimation and joint source-channel coding at the UE, and finally to the joint source-channel decoding and precoding design at the BS. Only one joint multi-module designed network is deployed at each device terminal.

- By jointly designing the pilot, CSI estimation, and CSI compression modules, the framework extracts task-relevant semantic information for transmission through end-to-end training, which indirectly reduces the source compression rate and improves feedback efficiency. Additionally, by avoiding explicit CE, the proposed JEFPNet decreases both storage and computational overhead at the UE.
- Performance comparisons between joint and separate architectures are conducted through simulation experiments. The results demonstrate the performance gains and stability of the joint architecture. The proposed JEFPNet proves to be more adaptive than separate architectures, particularly in the presence of large CSI estimation and feedback errors and is capable of designing more efficient precoding vectors than separate architecture.

The remainder of this paper is organized as follows: Section II introduces the system model for FDD MU-MIMO-OFDM systems and provides research background on AI-based CSI feedback to support this work. Section III describes the proposed framework, including the network architectures and end-to-end optimization objectives. Section IV presents the experimental results, and Section V concludes the paper.

Notations: In this paper, we denote Vectors and Matrices with boldface lower- and upper-case letters, respectively. \mathbf{A}^T and \mathbf{A}^H are transpose of \mathbf{A} and complex conjugate transpose operation of \mathbf{A} , respectively. a^* denotes the conjugate processing of complex variable a . $\|\cdot\|_2$ and $\|\cdot\|$ represents the ℓ_2 norm and modulus operations on complex numbers, respectively. $\mathbb{E}(\cdot)$ denotes the statistical expectation. $\{\cdot, \cdot\}$ denotes a set containing multiple elements. $\{\mathbf{A}_k\}_{k=1}^K$ denotes a set containing K elements from \mathbf{A}_1 to \mathbf{A}_K , and $\{\mathbf{A}(k)\}_{k=1}^K$ denotes a set containing K elements from $\mathbf{A}(1)$ to $\mathbf{A}(K)$. The symbols \mathbb{R} and \mathbb{C} represent sets of real and complex numbers, respectively. $\lfloor A \rfloor$ indicates the floor operation.

II. SYSTEM MODEL AND BACKGROUND

A. System Model

In this paper, we consider a MIMO OFDM system with K users, where each user is equipped with a single omnidirectional antenna, and the BS employs an array antenna with N_t elements. The system operates with N_c subcarriers. In this system, we simultaneously consider downlink CSI estimation, downlink CSI feedback in the uplink channel, and downlink precoding design. The downlink CSI of the k -th user can be expressed as $\mathbf{H}_d(k) \in \mathbb{C}^{N_c \times N_t}$, and the corresponding uplink feedback channel can be expressed as $\mathbf{H}_u(k) \in \mathbb{C}^{N_c \times N_t}$.

For the downlink CSI estimation phase, we consider the pilot-assisted CE method, that downlink CSI is estimated at the UE with the help of the known pilot sequence for transmitter and receiver. For the pilot sequence, in the time domain, we use sequential L OFDM symbols for CE. To reduce pilot overhead, pilots are placed at equal g intervals in the frequency domain, while the non-pilot positions are utilized for data or other channel control information transmission. M subcarriers are sampled at equal intervals g from the N_c subcarriers to place the pilots, and the indices of these subcarriers form the set of pilot sequences, denoted as $\mathcal{M} = \{\mathcal{M}_1, \dots, \mathcal{M}_M\} \in \mathbb{R}$, where $M = \lfloor N_c/g \rfloor$. In this paper, user interference during feedback is not considered. Consequently, the same pilot symbols are employed across different users. The pilot sequence at the \mathcal{M}_m -th subcarrier can be expressed as $\mathbf{P}_{\mathcal{M}_m} = [\mathbf{p}_{\mathcal{M}_m}^{(1)}, \dots, \mathbf{p}_{\mathcal{M}_m}^{(L)}] \in \mathbb{C}^{N_t \times L}$.

The received pilot signals at the \mathcal{M}_m -th subcarrier of the k -th user can be expressed as

$$\mathbf{y}_{\mathcal{M}_m}(k) = \mathbf{h}_{d,\mathcal{M}_m}^T(k) \mathbf{P}_{\mathcal{M}_m} + \mathbf{n}_{d,\mathcal{M}_m}(k) \in \mathbb{C}^{1 \times L}, \quad (1)$$

where $\mathbf{h}_{d,\mathcal{M}_m} \in \mathbb{C}^{N_t}$ denotes the \mathcal{M}_m -th subcarrier of downlink channel $\mathbf{H}_d = [\mathbf{h}_{d,1}, \dots, \mathbf{h}_{d,N_c}]^T$. $\mathbf{n}_{d,\mathcal{M}_m}(k)$ is downlink additive white Gaussian noise (AWGN) with mean zero and variance σ_{ce}^2 . In summary, the downlink pilot transmission process can be expressed as follows:

$$\mathbf{Y}(k) = \mathcal{F}_{ce,k}(\mathcal{P}), \quad (2)$$

where $\mathbf{Y}(k) = [\mathbf{y}_{\mathcal{M}_1}^T(k), \dots, \mathbf{y}_{\mathcal{M}_M}^T(k)]^T \in \mathbb{C}^{M \times L}$ represents the received pilot signal, and $\mathcal{P} = \{\mathbf{P}_{\mathcal{M}_m}\}_{m=1}^M$ presents all pilot symbols on the selected subcarrier and OFDM symbols. $\mathcal{F}_{ce,k}(\cdot)$ denotes the downlink pilot signal transmission process of the k -th user. Notably, the pilot sequence of each OFDM symbol satisfies the power constraint

$$\frac{1}{M} \sum_{\mathcal{M}_m \in \mathcal{M}} \|\mathbf{p}_{\mathcal{M}_m}^{(l)}\|_2^2 = 1. \quad (3)$$

With the channel normalization, the downlink signal-to-noise rate (SNR) during the CE phase can be expressed as

$$\text{SNR}_{ce} = \frac{1}{\sigma_{ce}^2}. \quad (4)$$

Using the received pilot signal $\mathbf{Y}(k)$ and the known pilot sequences \mathcal{P} , the downlink CSI of the k -th user can be estimated and subsequently compressed to obtain a semantic representation of the downlink CSI for reconstruction, denoted as

$$\mathbf{s}(k) = \mathcal{E}_\theta(\mathbf{Y}(k), \mathcal{P}) \in \mathbb{C}^Z, \quad (5)$$

where $\mathcal{E}_\theta(\cdot)$ denotes the processing at the UE side, including downlink CSI CE and CSI semantic information extraction, and θ denotes the set of trainable parameters for this process. Z denotes the number of feature elements, which also corresponds to the number of subcarriers occupied by the feedback after OFDM mapping. It is worth emphasizing that the output features satisfy the power constraints, as

$$\frac{1}{Z} \|\mathbf{s}(k)\|_2^2 = 1. \quad (6)$$

The received CSI semantic feature vector of the z -th subcarrier can be expressed as

$$\mathbf{y}_z(k) = \mathbf{h}_{u,z}^T(k) s_z(k) + \mathbf{n}_{u,z}(k) \in \mathbb{C}^{N_t}, \quad (7)$$

where $s_z(k)$ is the z -th element of $\mathbf{s}(k)$, and $\mathbf{h}_{u,z}(k) \in \mathbb{C}^{N_t}$ is z -th row of uplink channel $\mathbf{H}_u(k)$ for the k -th user. $\mathbf{n}_{u,z}(k)$ is uplink AWGN during the CSI feedback phase with zero mean and σ_u^2 variance. With the uplink noise power and transmission power constrain in Eq. (6), uplink feedback SNR can be expressed as

$$\text{SNR}_u = \frac{1}{\sigma_u^2}. \quad (8)$$

At the BS, we use an maximal ratio combining (MRC) receiver for detecting signals. The combining matrix is derived by the estimated uplink CSI. In this paper, we assume perfect uplink CE. Therefore, the combining matrix of the z -th subcarrier $\mathbf{W}_z(k)$ can be expressed as

$$\mathbf{W}_z(k) = \frac{\mathbf{h}_{u,z}(k)}{\|\mathbf{h}_{u,z}(k)\|_2}. \quad (9)$$

The detected semantic information $\hat{\mathbf{s}}(k)$ of downlink CSI can be expressed as

$$\hat{\mathbf{s}}_z(k) = \mathbf{W}_z^H(k) \mathbf{y}_z(k), \quad (10)$$

where $\hat{s}_z(k)$ represents the z -th element of the vector $\hat{\mathbf{s}}(k)$. The uplink CSI feedback process can be obtained with

$$\hat{\mathbf{s}}(k) = \mathcal{F}_{u,k}(\mathbf{s}(k)), \quad (11)$$

where $\mathcal{F}_{u,k}(\cdot)$ denotes uplink data transmission function of the k -th user.

The semantic feature information of downlink CSI from MU is aggregated at the BS. This aggregated downlink channel semantic feature information, encompassed from various users, is subsequently used to enable a joint precoding design in the MU scenarios. The operation at the BS can be expressed as follows:

$$\mathcal{V} = \mathcal{D}_\psi(\{\hat{\mathbf{s}}(k)\}_{k=1}^K), \quad (12)$$

where $\mathcal{V} = \{\mathbf{V}(k)\}_{k=1}^K$ represent the set of precoding matrices designed for different users, and $\mathbf{V}(k) = [\mathbf{v}_1(k), \dots, \mathbf{v}_{N_c}(k)]^T \in \mathbb{C}^{N_c \times N_t}$ denotes precoding matrix of the k -th user. $\mathcal{D}_\psi(\cdot)$ presents the process of downlink CSI reconstruction and precoding design with the trainable parameter set ψ at the BS side. It should be emphasized that the precoding matrices for different users satisfy the power constraint, as

$$\sum_{k=1}^K \|\mathbf{v}_{n_c}(k)\|_2^2 = P, \quad (13)$$

where the subscript $n_c \in \{1, \dots, N_c\}$ represents the n_c -th subcarriers, and P denotes downlink transmission power. The downlink transmit signal $x_{n_c}(k)$ of the k -th user at the n_c -th subcarrier after precoding process can be represented as $\mathbf{v}_{n_c}(k) x_{n_c}(k)$. With the transmit signals satisfying statistically independent and $\mathbb{E}\{x_{n_c}(k) x_{n_c}^*(k)\} = 1$, the SNR of the downlink channel after precoding process can be expressed as

$$\text{SNR}_d = \frac{P}{\sigma_d^2}. \quad (14)$$

$$R_{\theta,\psi,\mathcal{P}} = \sum_{k=1}^K \sum_{n_c=1}^{N_c} \log_2 \left(1 + \frac{\|\mathbf{h}_{d,n_c}^T(k) \mathbf{v}_{n_c}(k) x_{n_c}(k)\|^2}{\sum_{m \neq k} \|\mathbf{h}_{d,n_c}^T(k) \mathbf{v}_{n_c}(m) x_{n_c}(m)\|^2 + \sigma_d^2} \right). \quad (16)$$

Correspondingly, the received signal of the k -th user is

$$r_{n_c}(k) = \mathbf{h}_{d,n_c}^T(k) \sum_{k=1}^K \mathbf{v}_{n_c}(k) x_{n_c}(k) + n_{n_c}(k), \quad (15)$$

where $n_{n_c}(k)$ represents the downlink AWGN with power σ_d^2 during the data transmission phase. The downlink spectral efficiency is given in Eq. (16).

B. Background Description

The AI-based CSI feedback architecture can be classified into separate and joint architectures, as illustrated in Fig. 1. In the separate architecture, the AI network is designed to focus exclusively on source compression and reconstruction tasks, employing an end-to-end training approach that neglects the impact of channel coding and decoding on overall performance. As a consequence, when channel coding, decoding, and the communication channel are taken into account during testing, a phenomenon known as the ‘‘cliff effect’’ occurs. This effect arises when the channel quality deteriorates beyond the capacity of the channel coding, leading to a sharp decline in source reconstruction quality. This phenomenon will result in system performance degradation or retransmission delay. The root cause is the alteration of the input distribution to the source reconstruction module, as the inclusion of channel coding, decoding, and transmission changes the input characteristics. During training in the separate architecture, the output from the source compression module is directly fed into the source reconstruction module, maintaining consistency in the distributions between the outputs of the CSI compression module and the inputs of the CSI reconstruction module. However, during testing, if channel coding fails, significant errors are introduced into the inputs of the source reconstruction module, causing a mismatch between the input distribution observed during training and that encountered during testing, resulting in performance degradation.

In contrast, the joint architecture integrates source and channel coding into a unified module, allowing the network to adapt to changing channel conditions during training via an end-to-end approach. This integration effectively mitigates the ‘‘cliff effect’’ typically observed in separate architectures. The joint architecture has been successfully implemented in several of our previous works for the CSI feedback task [13], [18] and the image transmission task [6], demonstrating its efficacy. Consequently, the feedback mechanism in this paper also adopts this DJSCC framework.

III. DJSCC-BASED MU JOINT CHANNEL ESTIMATION, FEEDBACK, AND PRECODING DESIGN

In the MU MIMO-OFDM scenario, we propose an end-to-end joint estimation, feedback and precoding network (JEFP-

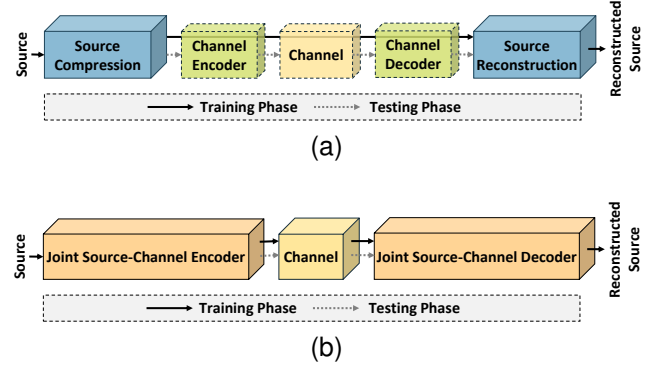


Fig. 1. Architectures of AI-based CSI feedback: (a) the separate architecture; (b) the joint architecture.

Net), as shown in Fig. 2, by considering the three processes of downlink CSI estimation, uplink CSI feedback under the DJSCC architecture, and downlink precoding design.

The downlink CE adopts the pilot-assisted CE algorithm, and the pilot symbols use trainable pilot symbols. A complex fully connected (FC) neural network architecture is employed to facilitate pilot design. Specifically, the complex-valued pilot parameters to be trained are separated into real and imaginary components. The real and imaginary parts of the pilot sequence for the \mathcal{M}_m -th subcarrier can then be expressed as $\mathcal{R}(\mathbf{P}_{\mathcal{M}_m})$ and $\mathcal{I}(\mathbf{P}_{\mathcal{M}_m})$. Similarly, the downlink channel and the received signal can be expressed in the same form, the real part of the received signal of the k -th user in the \mathcal{M}_m -th subcarrier can be expressed as

$$\begin{aligned} \mathcal{R}(\mathbf{y}_{\mathcal{M}_m}(k)) &= \mathcal{R}(\mathbf{h}_{d,\mathcal{M}_m}^T(k)) \mathcal{R}(\mathbf{P}_{\mathcal{M}_m}) - \\ &\quad \mathcal{I}(\mathbf{h}_{d,\mathcal{M}_m}^T(k)) \mathcal{I}(\mathbf{P}_{\mathcal{M}_m}) + \\ &\quad \mathcal{R}(\mathbf{n}_{d,\mathcal{M}_m}(k)), \end{aligned} \quad (17)$$

while the imaginary part can be expressed as

$$\begin{aligned} \mathcal{I}(\mathbf{y}_{\mathcal{M}_m}(k)) &= \mathcal{R}(\mathbf{h}_{d,\mathcal{M}_m}^T(k)) \mathcal{I}(\mathbf{P}_{\mathcal{M}_m}) + \\ &\quad \mathcal{I}(\mathbf{h}_{d,\mathcal{M}_m}^T(k)) \mathcal{R}(\mathbf{P}_{\mathcal{M}_m}) + \\ &\quad \mathcal{I}(\mathbf{n}_{d,\mathcal{M}_m}(k)). \end{aligned} \quad (18)$$

The received pilot signal vectors are concatenated in the frequency domain to form the received pilot matrix, denoted as $\mathbf{Y}(k)$ for the k -th user. Treating the real and imaginary parts as separate channels, this two-channel received pilot matrix is fed into the encoder module for direct compression. The network architecture of the encoder module is shown in Fig. 3. Here, ‘‘Conv $F|(W_1, W_2)|(S_1, S_2)$ ’’ indicates a convolutional layer with F filters, a window size is $W_1 \times W_2$, and a stride of $S_1 \times S_2$. ‘‘BN + LeakyReLU’’ represents a batch normalization (BN) layer followed by the ‘‘LeakyReLU’’ activation function. ‘‘Dense($2Z$)’’ denotes a FC layer with $2Z$ neurons.

$$\begin{aligned}
& \underset{\theta, \psi, \mathcal{P}}{\text{maximize}} R_{\theta, \psi, \mathcal{P}} = \sum_{k=1}^K \sum_{n_c=1}^{N_c} \log_2 \left(1 + \frac{\|\mathbf{h}_{d, n_c}^T(k) \mathbf{v}_{n_c}(k) x_{n_c}(k)\|^2}{\sum_{m \neq k} \|\mathbf{h}_{d, n_c}^T(k) \mathbf{v}_{n_c}(m) x_{n_c}(m)\|^2 + \sigma_d^2} \right) \\
& \text{s.t.} \quad \left\{ \{\mathbf{v}_{n_c}(k)\}_{n_c=1}^{N_c} \right\}_{k=1}^K = \mathcal{D}_{\psi} \left(\left\{ \mathcal{F}_{u, k}(\mathcal{E}_{\theta}(\mathcal{F}_{ce, k}(\mathcal{P}), \mathcal{P})) \right\}_{k=1}^K \right)
\end{aligned} \tag{19}$$

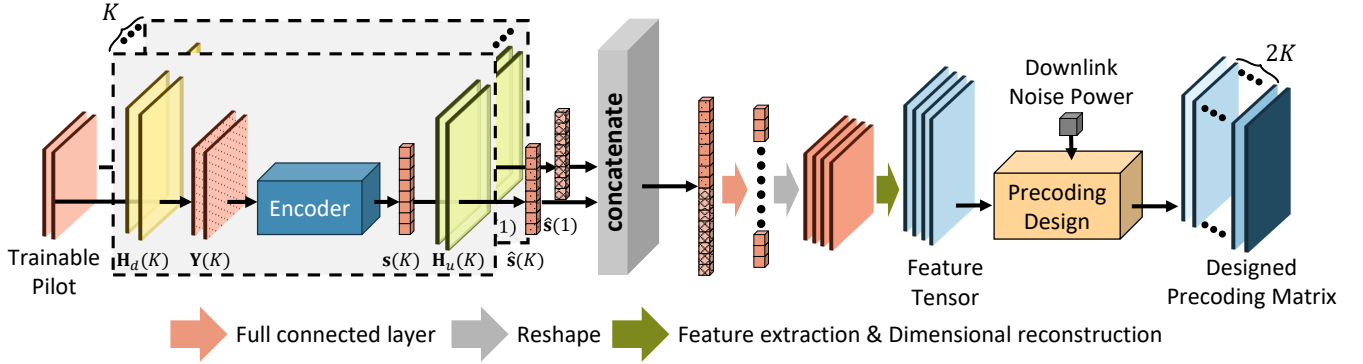


Fig. 2. Architecture of the JEFNet. (Certain parameter-free operations are omitted for simplicity.)

In the encoder module, CSI features are first extracted by the convolutional layer, then reshaped into vectors, and finally compressed into $2Z$ -dimensional vectors using an FC layer with $2Z$ neurons. The transmit power is fixed through power normalization and OFDM mapping of the feature vectors before transmission.

It is important to note that users are assumed to be located within the same cell, sharing similar scatterer environments and channel statistical parameters. Consequently, the downlink CSI of different users follows the same distribution, allowing us to use a single trainable pilot across users. Additionally, the encoder module parameters are also shared among other users, significantly reducing the number of training parameters and accelerating training convergence. This parameter-sharing strategy also eliminates the need for the BS to adjust the pilot sequences for different users. Additionally, the UE only needs to store the encoder parameters for a specified cell, or it can receive them directly from the BS without requiring a user identity document.

In this paper, we do not consider multiple access scenarios. We assume that each user feeds back CSI during a single OFDM symbol, with CSI feedback occurring sequentially for each user without inter-user interference during the feedback phase. The semantic feature vectors obtained from each user's compressed signal are concatenated into a vector of dimension $2KZ$ at the BS through a "Concatenation" layer after passing through individual channels in real number. Following this, an FC layer recovers the CSI dimension, transforming the vector of dimension $2KZ$ to one of dimension $2KMN_t$. A "Reshape" layer then converts this vector into a semantic feature tensor with dimensions $M \times N_t \times 2K$, where $2K$ represents the number of channels for this tensor. The feature tensor for each channel can thus be treated as a semantic feature matrix with M rows and N_t columns. This MU

CSI semantic feature tensor is processed by a convolutional network and a transposed convolutional network to extract features and reconstruct dimensions aligned with the dimensional requirements of precoding design. Finally, the resulting feature tensor, combined with downlink noise power, is fed into the precoding design module to complete the precoding design. The outputs of the precoding design module are the newly designed precoding matrix set for K users as shown in Eq. (12), each with N_t antennas and N_c subcarriers.

The entire network is trained in an end-to-end manner. Inputs to the network include the downlink full CSI for the CE phase and downlink data transmission phase, the uplink CSI for the feedback phase, and the SNR for each phase. The objective of network optimization is to maximize the downlink spectral efficiency, which can be expressed as Eq. (19)

A. Feature Extraction and Dimensional Reconstruction

By directly extracting the channel CSI for compression at the UE, the source compression rate is indirectly reduced. At the same time, both parameter storage and computational overhead are decreased, because the source data for compression is changed from full CSI to a received pilot signal with lower dimensionality. Since the compressed pilot signals have contained the required downlink CSI semantic information of users, a feature extraction network at the BS is used to capture MU CSI semantic features, and a dimensional reconstruction network is employed to reconstruct the feature dimensions.

The structure of the feature extraction and dimensional reconstruction networks is shown in Fig. 4. First, for the feature tensor of dimension, $M \times N_t \times 2K$, features are extracted using multiple residual blocks composed of convolutional layers, BN layers, and activation function layers. The dimensional reconstruction network employs I transposed convolutional layers to reconstruct low-dimensional features to

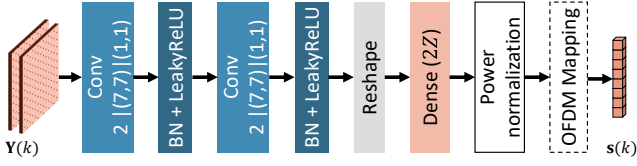


Fig. 3. Architecture of encoder module. Different users utilize encoders with shared parameters, meaning the input tensor and output vector do not include user-specific identifiers.

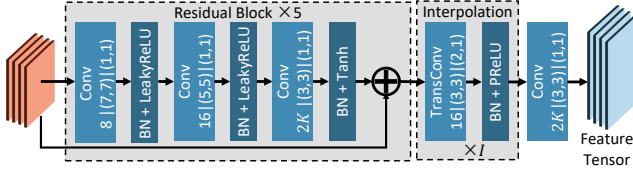


Fig. 4. Procession of feature extraction and dimensional reconstruction.

the target dimensionality of the precoding vector by adjusting the stride S_1 , followed by a convolutional layer to set the number of output feature channels. Overall, the dimensional transformation $M \times N_t \times 2K \rightarrow N_c \times N_t \times 2K$ is achieved by the dimensional reconstruction network.

B. Precoding Design

In the precoding design module, we account for the correlation between different subcarriers and employ a consistent network architecture and parameters for the precoding design across subcarriers to reduce both the number of training parameters and storage overhead. The input feature tensor is first concatenated along the user and antenna dimensions, then concatenated with the downlink noise power as known information to assist with power allocation. The concatenated vectors for each subcarrier contain the CSI of MU along with the downlink noise power, so precoding vectors for K users are designed using two FC layers and the tanh activation function, as shown in Fig 5. Note that a power normalization process must follow the last activation function layer to meet the power constraints in Eq. (13). Finally, the newly designed precoding matrix is reshaped to form a precoding tensor with dimensions: width corresponding to the number of BS antennas N_t , length to the number of subcarriers N_c , and channels to twice the number of users K (representing real and imaginary components). The set of precoding matrices for K users is then obtained by separating this tensor along the channel dimension, which is expressed as \mathcal{V} .

IV. EXPERIMENTAL RESULTS

In this paper, we propose an end-to-end JEFNet that incorporates three phases of CSI feedback, beginning at the UE and returning to the UE: downlink CSI estimation, uplink CSI feedback, and downlink precoding design. In this section, we demonstrate the effectiveness of the proposed network by comparing our algorithm with traditional algorithms through simulation experiments. We also verify the performance advantages of the end-to-end multi-module joint designed architecture by comparing the joint network architecture with

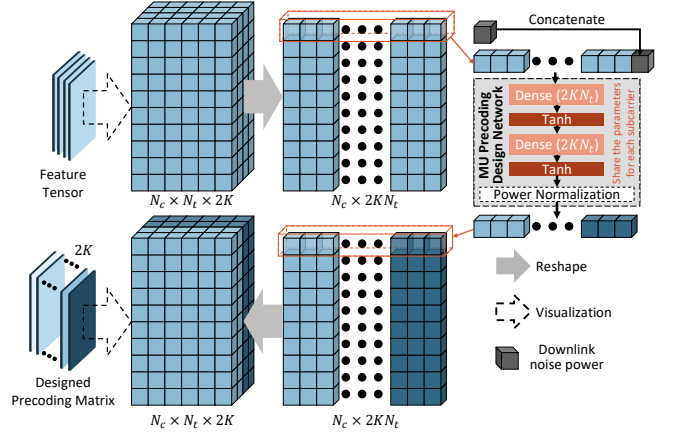


Fig. 5. Architecture of MU precoding design module. To facilitate understanding, we represent the feature tensor as a set of $N_c \times N_t \times 2K$ squares. Similarly, the precoding tensor is depicted as $N_c \times N_t \times 2K$ squares, with different colors used to distinguish the precoding tensor for different users, each characterized by $N_c \times N_t \times 2$.

the corresponding separate network architecture. Finally, we evaluate the scalability of the network with respect to varying feedback overhead and the number of supported users.

This paper considers a MU urban macro-cell (UMa) channel scenario to simulate the proposed network architecture. The users work in an FDD system with an uplink frequency of 2.1 GHz and a downlink frequency of 1.9 GHz. An OFDM system with $N_c = 96$ subcarriers and a 10 MHz bandwidth is employed for both uplink and downlink. The BS is equipped with $N_t = 32$ logical antenna ports, implemented using 8×8 dual-polarized physical surface array antennas, with the mapping between logical ports and physical antennas realized through a sparse matrix with power constraints. Each UE is equipped with a single omnidirectional antenna. Other antenna settings, user locations, and scenario configurations follow the 3rd Generation Partnership Project (3GPP) TR 38.901 standard [23].

In the downlink CE phase, sparse pilots with equal spacing are utilized, with a pilot interval of $g = 4$, corresponding $M = 24$. User locations are randomly distributed following the standard, and Quadriga [24] is used to generate the corresponding uplink and downlink CSI for each user. The uplink and downlink CSI of K users are aggregated to form one sample. The dataset comprises 100,000 training samples, 30,000 validation samples, and 20,000 test samples. Training is conducted over 500 epochs, utilizing the Adam optimizer with a batch size of 128. The initial learning rate is set to 0.001 and is reduced by half if the validation loss does not improve for 20 consecutive epochs. The downlink spectral efficiency is calculated with Eq. (16) under a downlink power constraint of $P = 1$.

A. Separate Architecture

To evaluate the performance differences between the joint and separate architectures, we designed a separate architecture comprising downlink CE, CSI compression, CSI reconstruction, and precoding design tasks, as shown in Fig. 6. At

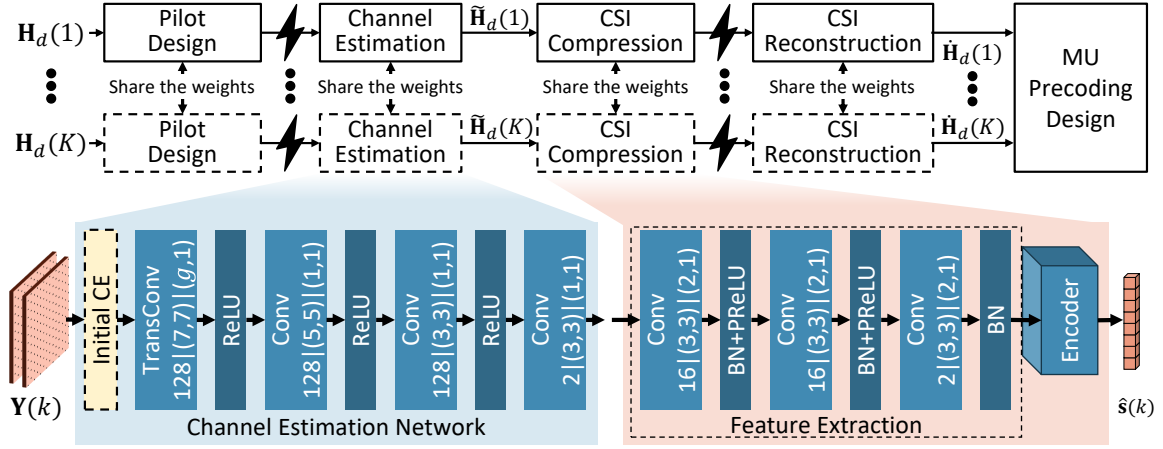


Fig. 6. The system model includes pilot design, CSI estimation, CSI feedback, and precoding design within a separate architecture framework. Additionally, network architecture diagrams for some modules not featured in the joint architecture are provided. For different users, the parameters are shared across modules because they operate in the same scatterer environment.

the UE, instead of the joint CE and CSI compression used in JEFNet, we first employ a CE network to estimate the downlink CSI. Next, a feature extraction network is applied to extract the downlink CSI features in the frequency domain, followed by CSI compression using the same architecture depicted in Fig. 3. The compressed CSI is then transmitted. The details of the CE network and the processing of downlink CSI feature extraction are both illustrated in Fig. 6. For the CE network, we begin by using the learnable parameter matrix $\mathbf{O}_{\mathcal{M}_m} \in \mathbb{C}^{L \times N_t}$ with the bias vector $\mathbf{b}_{\mathcal{M}_m} \in \mathbb{C}^{N_t}$ for each subcarrier posted pilots, i.e., $\mathcal{M}_m \in \mathcal{M}$ to simulate the linear minimum mean square error (LMMSE) CE, providing the initial estimation result [25]. Similar to the operation of the learnable pilot matrix, the real and imaginary parts of the received pilot signal $\mathbf{Y}(k)$ of the K -th user are processed separately, i.e., the real part of the initial estimated downlink CSI of the \mathcal{M}_m -th subcarrier can be expressed as $\mathcal{R}(\mathbf{y}_{\mathcal{M}_m}(k))\mathcal{R}(\mathbf{O}_{\mathcal{M}_m}) - \mathcal{I}(\mathbf{y}_{\mathcal{M}_m}(k))\mathcal{I}(\mathbf{O}_{\mathcal{M}_m}) + \mathcal{R}(\mathbf{b}_{\mathcal{M}_m})$, and the imaginary part can be expressed as $\mathcal{R}(\mathbf{y}_{\mathcal{M}_m}(k))\mathcal{I}(\mathbf{O}_{\mathcal{M}_m}) + \mathcal{I}(\mathbf{y}_{\mathcal{M}_m}(k))\mathcal{R}(\mathbf{O}_{\mathcal{M}_m}) + \mathcal{I}(\mathbf{b}_{\mathcal{M}_m})$. A transpose convolution layer is then employed to perform upsampling in the frequency domain, followed by several convolution layers and ReLU activation layers for feature extraction and channel reconstruction. As illustrated in Fig. 6, the feature extraction process consists of convolution and transpose convolution layers, along with batch normalization layers and activation functions.

At the BS, the downlink CSI is first reconstructed using a CSI reconstruction network, which employs an architecture similar to the decoder in [13]. The CSI of different users is processed using CSI reconstruction networks with the same parameters. Following CSI reconstruction, precoding vectors are designed based on the reconstructed CSI of the MU.

It is important to note that in the separate architecture, the modules performing distinct tasks are individually trained with optimization objectives tailored to their respective tasks and then integrated for end-to-end performance testing. For the downlink CSI estimation task, a pilot design and CE network

is utilized, and its loss function aims to maximize estimation accuracy, represented by

$$\mathcal{L}_{CE} = \text{minimize} \left\{ \text{MSE} \left(\mathbf{H}_d(k), \tilde{\mathbf{H}}_d(k) \right) \right\}, \quad (20)$$

where $\text{MSE}(\cdot)$ denotes the mean square error (MSE) between the two inputs. $\tilde{\mathbf{H}}_d(k)$ is the estimated downlink CSI of the k -th user as shown in Fig. 6

Similarly, the CSI compression and reconstruction network is employed for the CSI feedback task, and its training loss function maximizes reconstruction accuracy, which also can be expressed as

$$\mathcal{L}_{FB} = \text{minimize} \left\{ \text{MSE} \left(\mathbf{H}_d(k), \hat{\mathbf{H}}_d(k) \right) \right\}, \quad (21)$$

where $\hat{\mathbf{H}}_d(k)$ is the reconstructed downlink full CSI of the k -th user as shown in Fig. 6.

For the downlink precoding design processing, we consider two approaches: traditional precoding design and AI-based precoding design. In the traditional scheme, we employ the singular value decomposition (SVD) precoding method, which leverages the outputs, from $\tilde{\mathbf{H}}_d(1)$ to $\tilde{\mathbf{H}}_d(K)$, of the CSI reconstruction module for K users. The SVD algorithm is applied to different subcarriers to obtain the right singular vectors and eigenvalues for the K users. These right singular vectors are then used as the precoding vectors for transmitting the downlink data. Downlink power allocation is performed using the water-filling (WF) algorithm, which utilizes the eigenvalues and the downlink noise power σ_d^2 to determine the downlink transmission power for the K users. For the AI-based precoding design, we use the network architecture ideas as [18] to jointly design the CSI feedback and precoding design networks. Both the CSI feedback module and the precoding design module share the same network architecture as JEFNet to ensure a fair comparison. This approach is referred to as ‘‘JFPNet,’’ and its loss function is defined as maximizing the downlink spectral efficiency, using the ideally estimated CSI as the source for joint CSI feedback and precoding design.

TABLE I
IMPACT OF CE AND CSI FB ACCURACY ON THE PERFORMANCE OF
CONVENTIONAL SVD PRECODING ALGORITHMS

SNR_u	Ideal CE & FB	Ideal FB	Ideal CE	SVD & WF
-10 dB	14.405	6.687	3.923	3.874
-5 dB	14.405	6.687	4.372	4.275
0 dB	14.405	6.687	4.548	4.443
5 dB	14.405	6.687	4.611	4.505
10 dB	14.405	6.687	4.633	4.521

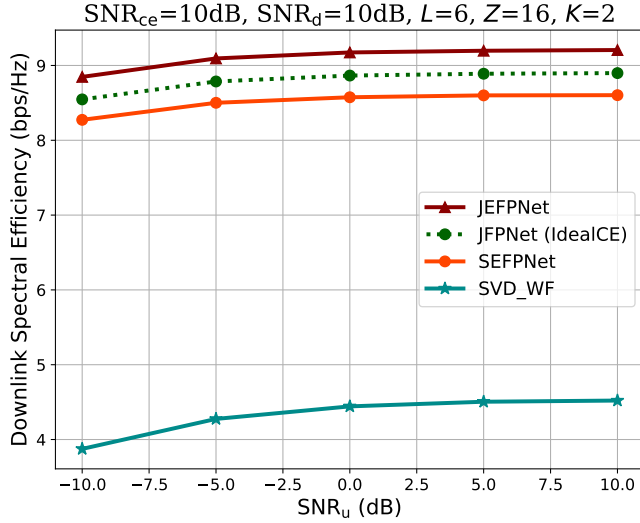


Fig. 7. Performance comparison of JEFNet with traditional separate architecture and partial separate architecture for CSI estimation, feedback, and precoding.

B. Performance Comparison Among Different Architecture

In this section, we compare the downlink spectral efficiencies of three different architectures: JEFNet in a joint architecture, SVD precoding with WF power allocation in a separate architecture, and JFPNet in a partially separate architecture. The experiments are carried out with the SNR_{ce} in the CE phase and the SNR_d in the downlink data transmission phase fixed. The number of CE symbols (L) is set to 6, the feedback overhead (Z) is 16, and the number of users (K) is 2. By varying the SNR of the uplink feedback channel, i.e. SNR_u , we evaluate the downlink spectral efficiency for each architecture. The experimental results are shown in Fig. 7. The curve labeled “JFPNet” depicts the JFPNet network architecture under ideal CE. The curve “SEFPNet” indicates the performance when the CE module is separately trained with JFPNet and tested together after concatenation. The “SVD_WF” curve represents the performance of the separate architecture, where the CE and CSI feedback modules are separately trained, and then concatenated for testing to generate reconstructed downlink CSI for precoding design with SVD and WF algorithms.

The experimental results show that, compared to traditional algorithms, represented by the “SVD_WF” curve in Fig. 7, the joint feedback and precoding design architecture consistently delivers performance gains. This is consistent with the findings of our previous work in [18]. Meanwhile, the proposed JEFNet architecture delivering superior performance.

At $\text{SNR}_u = -10$ dB, JEFNet achieves a performance gain of 4.97 bps/Hz over the traditional method depicted as the curve “SVD_WF,” and at $\text{SNR}_u = 10$ dB, the gain is 4.69 bps/Hz. Compared to the “SEFPNet,” which also account for CE and CSI feedback errors, JEFNet achieves a performance gain of approximately 0.57 bps / Hz at $\text{SNR}_u = -10$ dB and 0.60 bps/Hz at $\text{SNR}_u = 10$ dB.

Additionally, even when compared to “JFPNet,” which utilizes the ideal downlink full CSI as its source, the JEFNet architecture still demonstrates a performance gain of 0.30 bps/Hz at $\text{SNR}_u = -10$ dB. This improvement can be attributed to the joint estimation and feedback architecture employed by JEFNet. Although both “SEFPNet” and “JFPNet” utilize CSI compression networks similar to JEFNet, they compress the source using full CSI, while JEFNet compresses the source using a lower-dimensional pilot signal instead. As a result, JEFNet equivalently reduces the compression rate for the same output dimension. Meanwhile, with the assumption of limited transmission resources, directly extracting effective features from the received pilot signals with an end-to-end training manner with specific task objectives can enhance the efficiency of transmitting relevant semantic information, which in turn improves the downlink spectral efficiency.

To investigate the performance loss of traditional algorithms, we compare the effects of CE errors and CSI feedback errors on traditional precoding design, with the results summarized in Table I. The experimental configurations in Table I align with those in Fig. 7. In Table I, “Ideal CE & FB” refers to the case that SVD precoding and the WF algorithm are used with ideal CE and CSI feedback. “Ideal FB” represents the case where erroneous CE is used with ideal CSI feedback, alongside the SVD precoding method. “Ideal CE” indicates the case where only the effect of CSI feedback on the traditional precoding algorithm is considered. The results in Table I show that the CSI feedback errors have a significant impact on the performance of the traditional algorithm. Specifically, when the feedback overhead Z is 16 and the feedback channel quality SNR_u is -10 dB, CSI estimation errors lead to a performance degradation of 7.718 bps/Hz, while CSI feedback errors lead to a performance degradation of approximately 10.48 bps/Hz. Moreover, with the existence of CSI feedback errors, the addition of CE errors results in a performance loss of 0.049 bps/Hz. The smaller performance loss caused by CE error can be attributed to the large CE overhead (L) and the high SNR_{ce} of the downlink CE, both of which mitigate its impact, while the CSI feedback overhead remains relatively small. Nevertheless, the joint design of CSI feedback and precoding significantly reduces this performance loss, as demonstrated by the experimental results in Fig. 7 with curves “SEFPNet” and “JEFNet”.

C. Advantage of End-to-End Multi-Module Joint Training

JEFNet is trained in an end-to-end manner that incorporates CE errors into the optimization of network parameters. In this subsection, we investigate the impact of estimation overhead and the channel quality during the CE phase on the final performance metrics (downlink spectral efficiency)

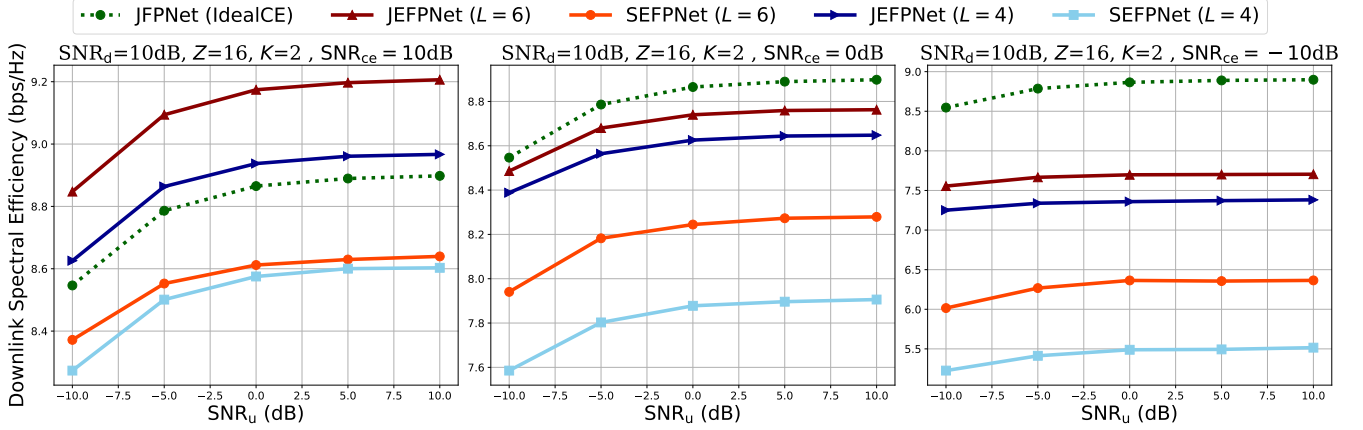


Fig. 8. Impact of different CE errors and overheads on the performance of separate and joint architectures.

of the network. The experimental results are presented in Fig. 8, where the three figures correspond to different channel qualities, i.e., $\text{SNR}_{ce} \in \{-10\text{dB}, 0\text{dB}, 10\text{dB}\}$. The impact of varying CE overheads on performance is also compared within each figure by considering two overhead values, $L = 4$ and $L = 6$, in our experiments.

From the experimental results in Fig. 8, we observe that as feedback overhead and channel SNR decrease, the performance of both the separate and joint architectures deteriorates. However, the performance of JEFNet under the joint architecture consistently outperforms than SEFPNet under the separate architecture. When SNR_{ce} is reduced from 10 dB to 0 dB, the performance of JEFNet decreases by only 0.362 bps/Hz at $\text{SNR}_u = -10$ dB for the $L = 6$ case, while SEFPNet experiences a more drop of 0.431 bps/Hz under the same conditions. As SNR_{ce} further decreases from 10 dB to -10 dB, the difference between the two architectures becomes even more pronounced. The performance of JEFNet decreases by 1.292 bps/Hz, while SEFPNet's performance significantly decreases by 2.357 bps/Hz.

The reduction in CE overhead also impacts the downlink spectral efficiency. For $\text{SNR}_{ce} = 0$ dB, when the CE overhead L is reduced from 6 to 4, the performance of JEFNet degrades by approximately 0.1 bps/Hz in the range of $\text{SNR}_u \in [-10\text{dB}, 10\text{dB}]$, whereas the performance of SEFPNet drops by about 0.36 bps/Hz.

The above phenomena can be attributed to the fact that SEFPNet uses ground-truth CSI for training. When the CE overhead is smaller, or the channel quality during estimation is poor, the CSI fed back during testing deviates more from the ground-truth CSI distribution, leading to degraded performance in the subsequent joint feedback and precoding design module.

D. Analysis of Storage and Computational Complexity Overhead

In this subsection, we analyze the training parameters and floating point operations (FLOPs) of different architectures under specific configurations: the number of feedbacks $Z = 16$,

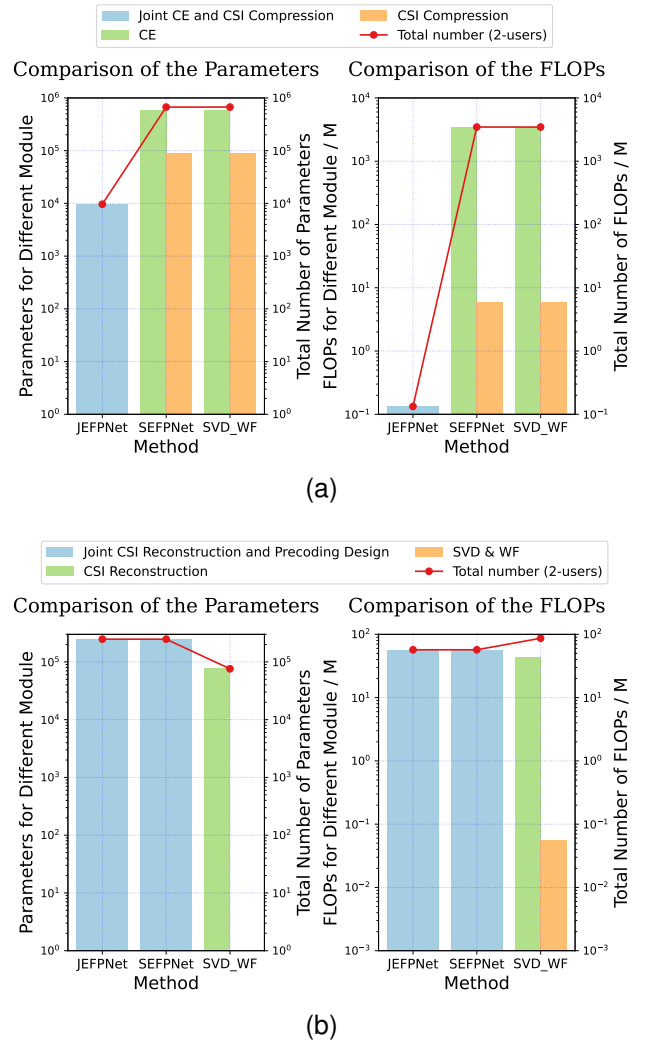


Fig. 9. Statistics on storage overhead and computational complexity for both sides of the communication system, considering different network architectures: (a) the UE side; (b) the BS side.

the number of subcarriers $N_c = 96$, the CE overhead $L = 6$, the pilot interval $g = 4$, and the number of users $K = 2$.

Fig. 9(a) illustrates the training parameters and FLOPs for

different modules at each UE side. Bar plots represent the parameters and FLOPs of every module, while line plots show the total parameters and FLOPs for every vendor. In the JEFNet architecture, the UE side consists only of a joint CE and CSI compression module, denoted as “Joint CE and CSI Compression”. In contrast, the partially separated SEFPNet and fully separated traditional architectures with SVD and WF algorithms, denoted as SVD_WF, implement CE and CSI compression as distinct modules, denoted as “CE” and “CSI Compression”, respectively. Statistical results reveal that the CE module in the separate architectures requires significantly more parameters and FLOPs. Additionally, the CSI compression module for feature extraction and CSI compression further increases the computational demand and parameter storage overhead. By comparison, the proposed JEFNet architecture requires only 1.44% of the parameters and 0.0038% of the FLOPs compared to the separate architectures, making it more suitable for hardware-constrained UEs.

Fig 9(b) displays the parameters and FLOPs at BS. Since JEFNet and SEFPNet share the same network architecture at the BS, their parameters and FLOPs, labeled as “Joint CSI Reconstruction and Precoding Design”, are identical. For the joint CSI reconstruction and precoding design module, since its network architecture depends on the number of users, both the parameters and FLOPs shown in Fig. 9(b) correspond to the case of two users. For the traditional architecture, CSI reconstruction at the BS is implemented using K decoders with shared parameters, labeled as “CSI Reconstruction”. Therefore, only one decoder’s parameters need to be stored and counted for statistics, which is shown on the left of Fig. 9(b). In the separate architecture, we employ SVD for precoding design and the WF algorithm for power allocation, collectively referred to as “SVD & WF”. Since the SVD and WF algorithms do not include trainable parameters, their parameter count is 0. For the FLOPs statistics shown on the right side of Fig. 9(b), the bar plot represents the FLOPs of every modular in the SVD_WF architecture, while the line plot corresponds to the total FLOPs at the BS vendor. As shown in Fig. 9(b), while the joint CSI reconstruction and precoding design in JEFNet requires 225.6% more training parameters than the separate architecture, it reduces FLOPs by 52.12%. The increase in storage overhead is not an issue for the BS equipped with sufficient hardware capabilities. Comparatively, the reduction in FLOPs decreases CSI feedback and precoding design latency, thereby enhancing precoding reliability and mitigating the effects of CSI aging.

E. Scalability Tests

In this subsection, we experimentally verify the scalability of the proposed network under varying feedback overheads and numbers of users. First, we fix the number of users (K) to 2, the SNR_{ce} of the CE phase to 10 dB, and the CE overhead (L) to 6. We compare the downlink spectral efficiencies of different network architectures with single-user CSI feedback overhead (Z) values of 8, 16, and 24. The experimental results, shown in Fig. 10, indicate that as feedback overhead increases, the downlink spectral efficiency for both joint and

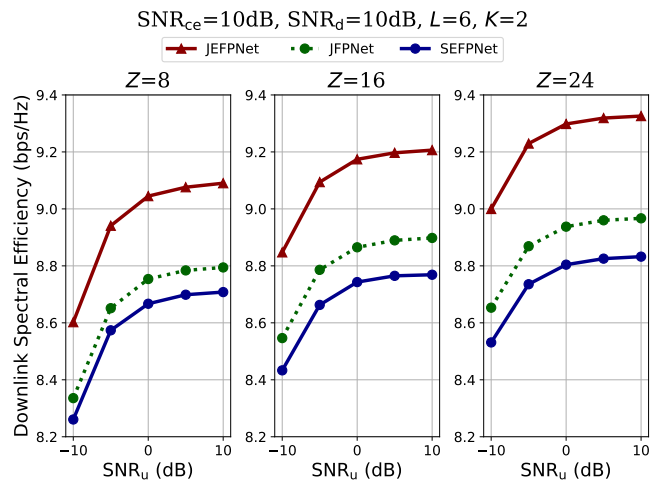


Fig. 10. Testing the downlink spectral efficiency of CSI estimation, feedback, and precoding design networks under partially separate and joint architectures as affected by the amount of feedback.

separate architectures gradually improves. Notably, JEFNet consistently outperforms JFPNet and SEFPNet. Specifically, the downlink spectral efficiency of JEFNet exceeds that of SEFPNet by 0.382 bps/Hz when $Z = 8$, 0.438 bps/Hz when $Z = 16$, and 0.494 bps/Hz when $Z = 24$, under $\text{SNR}_{\text{ce}} = 10$ dB.

Next, we fix SNR_{ce} to -10 dB, 0 dB, and 10 dB, the CE overhead to 6, and the feedback overhead to 32, while varying the number of users (K) between 2 and 3. The total transmit power P in the data transmission phase is limited to 1, irrespective of the number of users. As shown in Fig. 11, increasing the number of users results in higher downlink spectral efficiency. Our proposed JEFNet, implemented under the joint architecture, consistently outperforms SEFPNet, which operates under the separate architecture, particularly at low SNR_{ce} . When SNR_{u} is fixed at -10 dB and $K = 3$, the performance gain of JEFNet over SEFPNet is 0.815 bps/Hz at $\text{SNR}_{\text{ce}} = 10$ dB, 0.720 bps/Hz at $\text{SNR}_{\text{ce}} = 0$ dB, and 1.76 bps/Hz at $\text{SNR}_{\text{ce}} = -10$ dB. It is worth noting that, when $\text{SNR}_{\text{u}} = 0$ dB, the downlink spectral efficiency increases by 0.809 bps/Hz for three users compared to two users at $\text{SNR}_{\text{ce}} = -10$ dB, by 0.955 bps/Hz at $\text{SNR}_{\text{ce}} = 0$ dB, and by 1.02 bps/Hz at $\text{SNR}_{\text{ce}} = 10$ dB. This improvement is attributed to the higher SNR_{ce} during the CE phase, which enables the acquisition of more accurate downlink CSI semantic information with the limitation of feedback overhead and CE overhead, facilitating the design of precoding vectors that effectively eliminate inter-user interference.

V. CONCLUSION

In this paper, we propose an end-to-end architecture for CSI acquisition and precoding design in MU MIMO-OFDM systems, called JEFNet. At the UE side, a joint CSI estimation and compression network is proposed to compress and extract only the semantic information relevant to precoding from received pilot signals, rather than the entire CSI. This approach eliminates the overhead of explicit CE and indirectly reduces

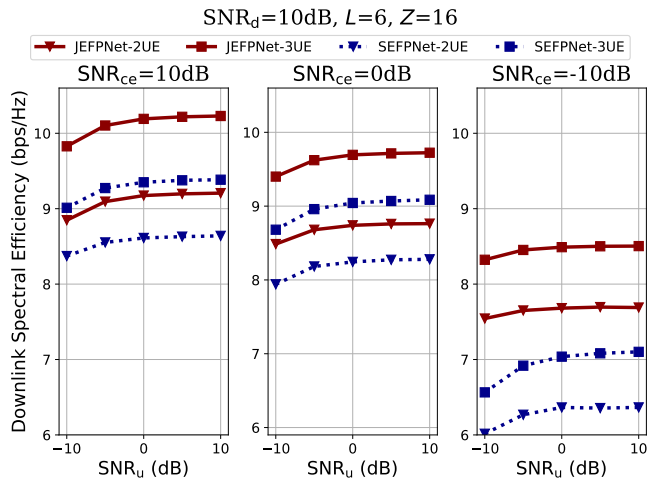


Fig. 11. Testing the scalability of the network architecture with a larger number of users.

the source compression rate to minimize information loss. At the BS, a proposed joint MU CSI reconstruction and precoding design network directly designs the precoding vectors from the received semantic information fed from each user. Additionally, a pilot learning matrix is employed at the BS to enhance the extraction efficiency of semantic information and maximize its utilization. The entire network is trained end-to-end with the objective of maximizing the downlink spectral efficiency. Multiple modules are jointly optimized to ensure that only semantic information related to the optimization objective is extracted and transmitted throughout the transmission process. Experimental results demonstrate that the proposed network achieves a higher downlink spectral efficiency under the same spectrum resource overhead. Furthermore, JEFNet significantly reduces both storage overhead and computational complexity at the UE side, which is more suitable for UE side without powerful storage capacity and computational ability. Simultaneously, it decreases computational complexity at the BS, reduces precoding design delay, and equips the network with the ability to counteract channel aging compared to separate architecture. Finally, we evaluate the scalability of the proposed network under varying feedback overheads and numbers of users, demonstrating that the performance of the network under the proposed joint architecture consistently outperforms that of the separate architecture.

REFERENCES

- [1] E. Björnson, C.-B. Chae, R. W. Heath, Jr., T. L. Marzetta, A. Mezghani, L. Sanguinetti, F. Rusek, M. R. Castellanos, D. Jun, and Ö. Tugfe Demir, "Towards 6G MIMO: Massive spatial multiplexing, dense arrays, and interplay between electromagnetics and processing," *arXiv e-prints*, p. arXiv:2401.02844, Jan. 2024.
- [2] Z. Wang, J. Zhang, H. Du, D. Niyato, S. Cui, B. Ai, M. Debbah, K. B. Letaief, and H. V. Poor, "A tutorial on extremely large-scale MIMO for 6G: Fundamentals, signal processing, and applications," *IEEE Commun. Surveys Tuts.*, vol. 26, no. 3, pp. 1560–1605, 2024.
- [3] S. Basharat, S. A. Hassan, H. Pervaiz, A. Mahmood, Z. Ding, and M. Gidlund, "Reconfigurable intelligent surfaces: Potentials, applications, and challenges for 6G wireless networks," *IEEE Wireless Commun.*, vol. 28, no. 6, pp. 184–191, 2021.
- [4] H. Chen, H. Sarriedden, T. Ballal, H. Wymeersch, M.-S. Alouini, and T. Y. Al-Naffouri, "A Tutorial on Terahertz-Band Localization for 6G Communication Systems," *IEEE Commun. Surveys Tuts.*, vol. 24, no. 3, pp. 1780–1815, 2022.
- [5] Z. Qin, J. Fan, Y. Liu, Y. Gao, and G. Y. Li, "Sparse representation for wireless communications: A compressive sensing approach," *IEEE Signal Process. Mag.*, vol. 35, no. 3, pp. 40–58, 2018.
- [6] J. Xu, B. Ai, W. Chen, A. Yang, P. Sun, and M. Rodrigues, "Wireless image transmission using deep source channel coding with attention modules," *IEEE Trans. Circuits Syst. Video Technol.*, vol. 32, no. 4, pp. 2315–2328, 2022.
- [7] W. Xu, Z. Yang, D. W. K. Ng, M. Levorato, Y. C. Eldar, and M. Debbah, "Edge learning for B5G networks with distributed signal processing: Semantic communication, edge computing, and wireless sensing," *IEEE J. Sel. Top. Signal Process.*, vol. 17, no. 1, pp. 9–39, 2023.
- [8] C.-K. Wen, W.-T. Shih, and S. Jin, "Deep learning for massive MIMO CSI feedback," *IEEE Wireless Commun. Lett.*, vol. 7, no. 5, pp. 748–751, 2018.
- [9] J. Guo, C.-K. Wen, S. Jin, and G. Y. Li, "Overview of deep learning-based CSI feedback in massive MIMO systems," *IEEE Trans. Commun.*, vol. 70, no. 12, pp. 8017–8045, 2022.
- [10] —, "Convolutional neural network-based multiple-rate compressive sensing for massive MIMO CSI feedback: Design, simulation, and analysis," *IEEE Trans. Wireless Commun.*, vol. 19, no. 4, pp. 2827–2840, 2020.
- [11] J. Cheng, W. Chen, J. Xu, Y. Guo, L. Li, and B. Ai, "Swin transformer-based CSI feedback for massive MIMO," in *2023 IEEE 23rd International Conference on Communication Technology (ICCT)*, 2023, pp. 809–814.
- [12] H. Ju, S. Jeong, S. Kim, B. Lee, and B. Shim, "Transformer-assisted parametric CSI feedback for mmWave massive MIMO systems," *IEEE Trans. Wireless Commun.*, vol. 23, no. 12, pp. 18774–18787, 2024.
- [13] J. Xu, B. Ai, N. Wang, and W. Chen, "Deep joint source-channel coding for CSI feedback: An end-to-end approach," *IEEE J. Sel. Areas Commun.*, vol. 41, no. 1, pp. 260–273, 2023.
- [14] Y. Guo, W. Chen, F. Sun, J. Cheng, M. Matthaiou, and B. Ai, "Deep learning for CSI feedback: One-sided model and joint multi-module learning perspectives," *IEEE Commun. Mag.*, pp. 1–8, 2024, early access, doi: 10.1109/MCOM.001.2400285.
- [15] M. Chen, J. Guo, C.-K. Wen, S. Jin, G. Y. Li, and A. Yang, "Deep learning-based implicit CSI feedback in massive MIMO," *IEEE Trans. Commun.*, vol. 70, no. 2, pp. 935–950, 2022.
- [16] J. Guo, C.-K. Wen, M. Chen, and S. Jin, "Environment knowledge-aided massive MIMO feedback codebook enhancement using artificial intelligence," *IEEE Trans. Commun.*, vol. 70, no. 7, pp. 4527–4542, Jul. 2022.
- [17] W. Chen, W. Wan, S. Wang, P. Sun, G. Y. Li, and B. Ai, "CSI-PPPNet: A one-sided one-for-all deep learning framework for massive MIMO CSI feedback," *IEEE Trans. Wireless Commun.*, vol. 23, no. 7, pp. 7599–7611, Jul. 2024.
- [18] Y. Guo, W. Chen, J. Xu, L. Li, and B. Ai, "Deep joint CSI feedback and multiuser precoding for MIMO OFDM systems," *IEEE Trans. Veh. Technol.*, vol. 74, no. 1, pp. 1730–1735, 2025.
- [19] J. Jee and H. Park, "Deep learning-based joint optimization of closed-loop FDD mmWave massive MIMO: Pilot adaptation, CSI feedback, and beamforming," *IEEE Trans. Veh. Technol.*, vol. 73, no. 3, pp. 4019–4034, 2024.
- [20] J. Guo, T. Chen, S. Jin, G. Y. Li, X. Wang, and X. Hou, "Deep learning for joint channel estimation and feedback in massive MIMO systems," *Digital Commun. Networks*, vol. 10, no. 1, pp. 83–93, Mar. 2024. [Online]. Available: <https://www.sciencedirect.com/science/article/pii/S235286482300024X>
- [21] F. Carpi, S. Venkatesan, J. Du, H. Viswanathan, S. Garg, and E. Erkip, "Precoding-oriented massive MIMO CSI feedback design," in *ICC 2023 - IEEE International Conference on Communications*, 2023, pp. 4973–4978.
- [22] F. Sohrabi, K. M. Attiah, and W. Yu, "Deep learning for distributed channel feedback and multiuser precoding in FDD massive MIMO," *IEEE Trans. Wireless Commun.*, vol. 20, no. 7, pp. 4044–4057, 2021.
- [23] 3GPP, "5G study on channel model for frequencies from 0.5 to 100 GHz," 3rd Generation Partnership Project (3GPP), Technical Specification (TS) 38.901, 2020, version 16.1.0.
- [24] S. Jaeckel, L. Raschkowski, K. Borner, and L. Thiele, "QuaDRiGa-quasi deterministic radio channel generator, user manual and documentation," *Fraunhofer Heinrich Hertz Institute, Tech. Rep. v2.6.1.*, 2021.

- [25] M. B. Mashhadi and D. Gündüz, “Pruning the pilots: Deep learning-based pilot design and channel estimation for MIMO-OFDM systems,” *IEEE Trans. Wireless Commun.*, vol. 20, no. 10, pp. 6315–6328, 2021.